Low-energy electron scattering from C_3H_4 isomers: Differential cross sections for elastic scattering and vibrational excitation

Yuichi Nakano, Masamitsu Hoshino, Masashi Kitajima, and Hiroshi Tanaka
Department of Physics, Sophia University, Tokyo 102-8854, Japan

Mineo Kimura
Graduate School of Science and Engineering, Yamaguchi University, Yamaguchi 755-8611, Japan
(Received 4 October 2001; published 23 September 2002)

Absolute differential cross sections (DCSs) for elastic and vibrationally inelastic scattering of electrons from C_3H_4 isomers (allene and propyne) have been determined by a crossed-beam experiment in the energy range 1.5–100 eV and over the scattering angles between 15°–130°. The relative flow method was applied to normalize these cross sections, using helium as a standard. Clear evidence of the strong isomer effect has been observed in DCSs for both elastic and vibrational excitation processes, and the isomer effect still conspicuously persists in total elastic cross sections. Two resonance regions where the vibrational cross sections are strongly enhanced are observed in both allene and propyne below a few eV, while both the DCSs become identical at higher energies, hence weakening the isomer effect. More details of the observed mode selectivity are discussed based on the selection rules for vibrational excitation via a shape resonance as well as on an argument based on the angular correlation.

DOI: 10.1103/PhysRevA.66.032714 PACS number(s): 34.80.−i, 34.50.−s, 34.10.+x

I. INTRODUCTION

For hydrocarbon molecules, as the number of carbon atoms increases, in general, the number of isomers increases even faster. However, the C_3H_4 molecule is known to possess two stable isometric-molecular structures, i.e., allene (propadiene; $H_2C{=}C{=}CH_2$, two double bonds), and propyne (methylacetylene; $HC{\equiv}C{-}CH_3$, triple and single bonds). It is obvious that isomers always show conspicuous differences in various physical and chemical properties, but it would be important to investigate for understanding the degree of the effect of the molecular structure and hence, electronic structure of the isomers. This would allow us to provide the general guideline of systematic understanding of dependence of electron-scattering dynamics to molecules.

As a part of a series of experimental studies for determining absolute cross sections by electron impact, we extend our previous investigations for the isomers of C_3H_6 [1]. In the present study, we intend to elucidate the bonding effect of the isomers, and compare these with the prototypes of the most simplest double-and triple-bond molecules such as C_2H_4 ($H_2C{=}CH_2$, a double bond) [2,3] and C_2H_2 ($HC{\equiv}CH$, a triple bond) [4,5] although these earlier studies did not particularly shed light on the isomer effects. To our knowledge, there are only a few experimental works available on two *cis*-and *trans*-isomeric structures of the $2n$-butene C_4H_8 by low-energy electron-impact spectroscopy [6–9]. But, no quantitative differential cross sections (DCSs) of the two isomers of C_3H_4 have been measured, and furthermore, they have not been compared with the elastic scattering and vibrational excitation from a viewpoint of the isomer. Recently, Deutsch *et al.* [10] have measured electron-impact ionization cross sections of two isomers of C_3H_6 (cyclopropane and propene), and have claimed that contrary to the earlier report [11], they have not seen any sizable isomer effect in ionization processes. Hence, it is interesting and in fact important to study the isomer effect in other processes at different energy regimes.

In the 1970s, Kuppermann and co-workers studied extensively allene [12] and propyne [13] by the electron-impact spectroscopy. In these papers, the history of investigation of both the optical-absorption and the electron-scattering experiments has been well described. But, almost all earlier investigations including these have only focused on the assignment of electronic excitations when compared to the optical absorption and the theoretical data, except that of Dance and Walker [8] and Van Veen and Plantenga [14] who have studied vibrational excitation of the ground electronic state via temporary negative-ion formation.

In this paper, absolute DCSs for elastic scattering and vibrational excitation are presented in the incident electron energy range from 1.5 to 100 eV and for detection angles from 15° to 130°. In addition, some details of the observed mode selection in the vibrational excitation are briefly discussed from the point of view of applying the angular-correlation theory of Andrick and Read [15]. Theoretical results for elastic cross sections are compared with the present measurements.

II. EXPERIMENTAL AND THEORETICAL APPROACHES

A. Experimental methods

The experimental arrangement and procedure used in the present DCS measurements were similar to those in previous studies [16]. Briefly, electrons from a 180° monochromator intercept an effusive molecular beam at right angles, and scattered electrons are energy analyzed in a second 180° spherical system. A number of tube lenses in the spectrometer have been used for imaging and energy control of the electron beam whose characteristics were confirmed care-

 ©2002 The American Physical Society

TABLE I. Molecular properties of allene and propyne [20].

Allene		Propyne	
Molecular structures			
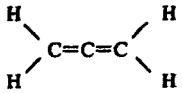		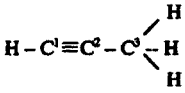	
D_{2d} symmetry		C_{3v} symmetry	
Bond length (Å) and angles			
C—H	1.071	C^3—H	1.112
C—C	1.335	C^1—H	1.060
		C^3—C^2	1.458
		C^2—C^1	1.207
∠H—C—H	113° ± 1°	∠H—C^3—H	108.4°
Dipole moment (D)			
0.2		0.77	

fully by electron trajectory calculations. To keep the transmission of the electrons constant in the lens system, the programmable power supplies control the driving voltages of some lenses. Both the monochromator and the analyzer are enclosed in differentially pumped boxes to reduce the effect of the background gases and to minimize the stray electron background. The target molecular beam is produced by effusing C_3H_4 through a simple nozzle with an internal diameter of 0.3 mm and a length of 5 mm. The spectrometer and the nozzle are heated to a temperature of about 50 °C to reduce any possibility of contamination during the measurements. The analyzer can be rotated around the scattering center covering an angular range from $-10°$ to 130° with respect to the incident electron beam. The overall energy resolution of the present measurements was 35–40 meV, and the angular resolution was $\pm 1.5°$. This energy resolution is not sufficient to resolve rotational excitations or individual vibrational modes (including the 11 and 10 fundamental modes and their overtones for allene and propyne). However, within the limited energy resolution, three compound peaks are observed at 0.12 eV (C—H bending vibrations, mainly, ν_4), 0.24 eV (C—C stretching vibrations ν_6), and 0.38 eV (C—H stretching vibrations $\nu_1+\nu_5+\nu_8$) in allene. Only two weak peaks are separated from the elastic peak at 0.17 eV (C—H bending, mainly, ν_4), 0.27 eV (C≡C stretching, mainly, ν_3), and 0.37 eV (C—H stretching ν_6) in propyne. Because many vibrational transitions in the peaks overlap, a deconvoluting procedure was employed to determine the cross sections for the individual transitions. Higher harmonics and mixed vibrational transitions have been neglected because the difficulties can be avoided. Absolute cross sections were obtained by the relative flow technique [17] using helium as the comparison gas. The geometrical length of the molecules is roughly 3.85 Å for allene and 4.84 Å for propyne, respectively, although their widths are comparable in size (1.79 Å vs 1.80 Å) (see Table I for molecular properties). The densities for the two gases are assumed to be identical by adjusting the pressure behind the nozzle so as to maintain approximately equal gas Knudsen numbers. The inelastic cross sections are normalized to the elastic ones by using the measured inelastic to elastic intensity ratios. The electron energy scale was calibrated with respect to the 19.367 eV resonance in He, and, for vibrational excitation, to the $^2\Sigma_g$ resonance of N_2. Experimental errors are estimated to be, at most, 15–20 % for the elastic DCSs and 30% for the vibrational and electronic excitation cross sections. The purity of gases used is 96% for allene and 98% for propyne, in addition to that of He with 99.999 95% [18]. We believe that the major part of impurities in allene and propyne come from another isomer.

The scattering spectrometer is operated in two ways. For the measurements of the angular dependence for the excitation processes, the intensity of the scattered electron signal is counted as a function of energy loss at a fixed impact energy and scattering angle. To study resonances in vibrational excitations, for instance, the analyzer is set to transmit only signals corresponding to a specific energy-loss channel as a function of impact energy.

B. Theoretical model

The theoretical approach employed is the continuum multiple-scattering (CMS) method, which is an efficient model for treating electron scattering in polyatomic molecules [19]. In short, the CMS divides the configuration space into three regions: region I, the atomic region surrounding each atomic sphere (spherical potentials), region II, the interstitial region (a constant potential), and region III, the outer region surrounding the molecule. The scattering part of the method is based on the static exchange with the asymptotic dipole-potential model within the fixed-nuclei approximation. The static interaction is constructed by the electron density obtained from the CMS wave function, and the Hara-type free-electron gas model [6] is employed for the local-exchange interaction, while the dipole interaction is considered for only terms proportional to r^{-2}.

With these assumptions, the Schrödinger equation in each region is solved numerically under separate boundary conditions. By matching the wave functions and their derivatives from each region, we can determine the total wave functions of the scattered electron, the scattering S matrix, and hence, the scattering cross section. This approach has been tested extensively and is known to provide useful information on the underlying scattering physics. Further, the CMS method is useful for interpolation and extrapolation for guiding experimental data points.

III. RESULTS AND DISCUSSION

Molecular structures and corresponding properties of allene and propyne are listed in Table I [20].

Allene is the simplest example of a cumulate or adjacent carbon-carbon double-bond system. The ground electronic state is nonplanar with the CH_2 planes at 90° to each other. The molecule then belongs to the D_{2d} point group with the X^1A_1 symmetry in the ground electronic state. Its ground-state electron configuration is $(1a_1)^2(1b_2)^2(2a_1)^2(3a_1)^2$

$(2b_2)^2(4a_1)^2(3b_2)^2(1e)^4(2e)^4(3e)^0(5a_1)^0$, yielding the lowest unoccupied orbitals $3e$ ($\pi a^*, \pi b^*$). The $2e$ and $3e$ molecular orbitals are each composed of two accidentally degenerate π or π^* orbitals, respectively, thus four pairs of excited states can be expected. According to Mosher, Flicker, and Kuppermann [12], two transitions with maxima at 4.28 and 4.89 eV were identified as singlet → triplet excitations ($2e \rightarrow 3e$; $1\ ^3A_1$ and $1\ ^3B_2$) with splitting due to the interaction between the two perpendicular molecular orbitals. The next low-lying transitions were also observed between 5.0 and 6.5 eV, and identified as spin-allowed but symmetry-forbidden transitions ($2e \rightarrow 3e$; $1\ ^1A_1$ and $1\ ^1B_2$). Furthermore, a weak singlet→singlet transition near 6.74 eV was attributed to an electric-dipole-allowed $X\ ^1A_1 \rightarrow 1\ ^1E$ transition. The 11 vibrational fundamental modes are classified in the symmetry types $\Gamma_{\text{vib}} = 3a_1 + b_1 + 3b_2 + 4e$, according to Shimanouchi's notation [21].

Propyne is a hydrocarbon molecule with a triple bond, and one of the derivatives of acetylene. The molecule belongs to the $C_{3\nu}$ point group with the $X\ ^1A_1$ symmetry in the ground electronic state. Its ground-state electron configuration is

$$(1a_1)^2(1b_2)^2(2a_1)^2(3a_1)^2(2b_2)^2(4a_1)^2(3b_2)^2(1e)^4.$$

According to earlier works [8,13,22], shape resonance with some oscillatory structures was observed at 3 eV, more than 1 eV above the corresponding resonance in C_2H_2. Two transitions ($a\ ^3\Sigma^+$ and $b\ ^3\Delta$:$2e \rightarrow 3e$) lying below the onset of optical excitation were detected and assigned as triplets at energies of 5.2 and 5.8 eV. The optically allowed transition at 6.7 eV was due to a singlet valence excited state (A; $^{1,3}\Sigma$:$2e \rightarrow 3e$), and also two other states were assigned as singlet transitions B and C ($^1\Delta$:$2e \rightarrow ns\sigma$) at 7.0 and 7.2 eV, respectively. The 10 vibrational fundamental modes are classified in the symmetry types $\Gamma_{\text{vib}} = 5a_1 + 5e$, according to the Shimanouchi's notation [21]. Both allene and propyne are weakly polar molecules, and as shown, display characteristic features of polar molecules in DCSs, i.e., sharp increase in DCSs particularly at smaller scattering angles.

A. Elastic scattering

1. DCSs for allene

Figure 1 shows absolute DCSs for allene in the incident energy range of 1.5–100 eV and for scattering angles between 15°–130°. The DCSs include vibrational excitation at 0.044 eV for the CCC deformation motion (ν_{11}) due to the limitation of the energy resolution in the present measurements. At 1.5 eV, the DCS shows a weak *d*-wave character that has a shallow minimum at 60° followed by a local maximum around 90° and a slightly depressed part at 120°. Because allene is a homopolar molecule, it may be suitable to represent that the DCS tends to drop in the backward scattering rather than to increase toward the forward scattering for the following reason. According to the application of modified effective-range theory to electron-polyatomic molecule (C_2H_6) scattering as discussed fully by Merz and Linder [23], the cross section is isotropic and dominated by the *s* wave only near zero energy. As the energy increases slightly to 5 meV, the angular dependences show that the backward scattering decreases to be half the value of the forward scattering, i.e., a typical *p*-wave character. Note that in the case of C_2H_6 the contributions from the quadrupole and anisotropic part of the polarizability are negligibly small. The forward scattering becomes dominant by increasing the energy in increments of 0.5 eV, where a resonant enhancement has been observed in the vibrational excitation at 2.1 eV as will be seen in Sec. III B below. As the energy increases to 2–3 eV, the angular dependence changes to decreasing trend toward smaller angles around the 20°–40° region and the maximum shifts to smaller angles. At 5 eV, the DCS becomes more isotropic, i.e., the forward scattering has a tendency to increase and a weak minimum appears around 120°. With further increase in the energy, the DCSs show common angular behavior, i.e., a steep increase toward smaller scattering angles followed a broad minimum at 90°. The new, but small hump, which shows up at 15 eV begins to shift toward smaller angles as the energy rises. At 100 eV, undulations in the DCS becomes apparent at the forward scattering side, which has been observed in other cumulate hydrocarbons and fluorocarbons such as C_3H_8, C_3F_8, OCS, and so on due to the interferences of the scattering waves from the composite atoms in the molecules.

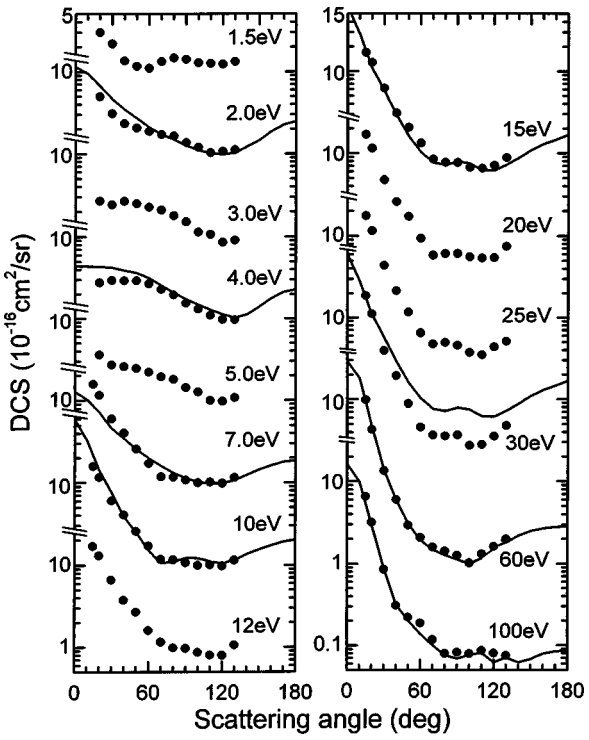

FIG. 1. Experimental (●) and calculated (–) DCSs for elastic scattering in allene.

2. DCSs for propyne

Figure 2 shows absolute DCS for propyne in the incident energy range of 1.5–100 eV and a scattering angle of 15°–130°. The DCSs also include vibrational excitation at 0.041 eV for the CCC bending motion (ν_{10}), due to the limitation

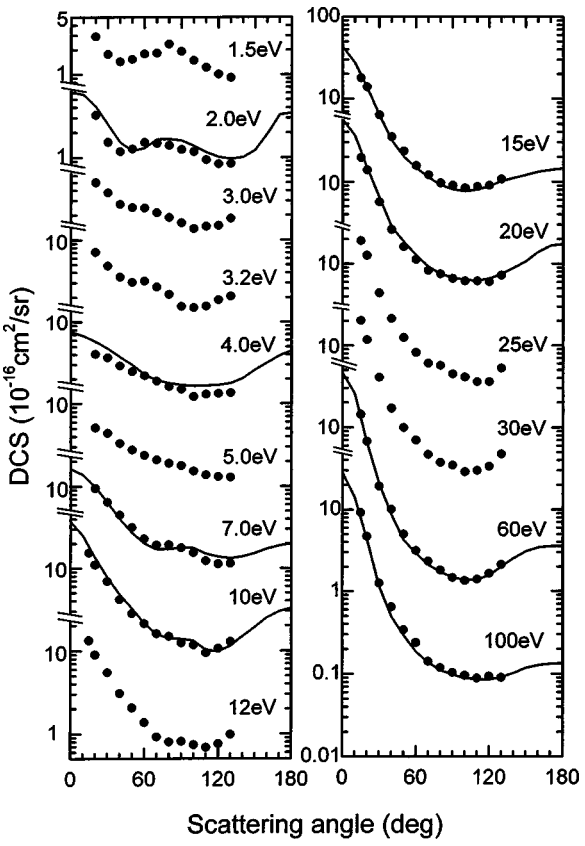

FIG. 2. Experimental (●) and calculated (–) DCSs for elastic scattering in propyne.

of the energy resolution in the present measurements. Compared to allene as shown above, at 1.5 eV a shallow minimum shifts to a lower scattering angle (40°) and a maximum near 80° is pronounced, a *d*-wave character being clear. Its *d*-wave characteristic shape is quite similar to the elastic C_2H_2 and N_2 cross sections, which are isoelectronic to each other. With slightly increase of the energy, the DCSs become gentle but the forward scattering is still dominant at both 2 and 3 eV due to the permanent dipole moment although weak. A weak hump emerges at 3.2 eV due to a shape resonance, which is located around 60° (as will be shown in Sec. III B). With a further increase in the energy, the DCSs show no undulation as a function of the scattering angles, showing a monotonic increase toward the zero scattering angle at 4 and 5 eV. Again, a weak structure shows up around 90° with shallow dints near 70° and 120° at 7.0 eV. This energy corresponds to the position of a weak resonant scattering process, which enhances the vibrational excitation (see in Sec. III B). Above 10 eV, the angular dependence is similar to those of allene in general, i.e., a steep increase toward lowering scattering angles followed a broad minimum at 90°. However, the DCSs become less structured in the overall scattering angles compared with those of allene. Moreover, both allene and propyne show some angular characteristics below 4 eV, which have been attributed partially to the resonance through the trapping of the incident electron in an low-lying orbital (a temporary negative ion, for simplicity called TNI). In elastic scattering a characteristic resonant feature is normally somewhat weakened, because the scattering results in the sum of resonant and nonresonant contributions. Contrasting to this, the resonances are more clearly visible in the inelastic scattering such as vibrational excitation as will be discussed in Sec. III B.

Hence, with the exception of the DCSs from 1.5 to 5 eV, it is concluded that the angular dependences for allene and propyne are very similar to each other although minor differences do exist.

The present CMS results for elastic DCSs for both molecules are included in Figs. 1 and 2. General agreement between the theory and the measured result is found to be reasonably good in the entire energy range, although their degree of agreement becomes somewhat better as the impact energy further increases. Regarding the experimental results, the CMS results clearly show several structures attributable to resonances below 5 eV. Particularly in 1–2 eV region, the relatively strong feature is observed. The theoretical result well reproduces this feature attributable to the *d*-wave character of the resonance.

3. Isomer effect

As apparent, the present DCSs for allene and propyne are well distinguishable from each other particularly for small-angle scattering at lower energies. For example, at 3 eV, the DCS below 40° for propyne tends to increase at much higher rate than that for allene due to the larger dipole moment. At 5 eV, the DCS for the allene shows the more pronounced feature typical to the *d*-wave resonance, while that for the propyne is more like *p*-wave shape. As the impact energy increases to 30 eV, both DCSs becomes nearly identical. Hence, contrary to impact ionization study of Ref. [10], the strong isomer effect for elastic scattering is observable at low energies. Even for ionization process, we believe that if one tries to measure ionization near threshold, then the isomer effect is expected to emerge because an ionized electron has sufficient time to interact with the molecular field before it escapes, and hence, it will be influenced by details of the difference of geometrical molecular structures and electronic states of the target.

4. Comparison with C_2H_2 and C_2H_4 vs propyne and allene: The bonding effect

Since allene and propyne have double and triple bond, respectively, it may be interesting to examine if the any fingerprint of the bonding effect on DCSs will appear in comparison with other hydrocarbons of the same number of the bonds. C_2H_2 and C_2H_4 molecules have a double and triple bond and hence, one may expect these to be good candidates for this comparative study. Figures 3 and 4 depict DCSs for allene vs C_2H_4, and propyne vs C_2H_2, respectively. Above 20 eV and in the range 40°–50°, DCSs for allene and C_2H_4, and propyne and C_2H_2 agree very well each other, while small but non-negligible discrepancies begin to appear at smaller scattering angles below 40°. For large scattering events, the incident electron should penetrate inside the target, and this in turn receives stronger influence from the molecular region where the electron density concentrates,

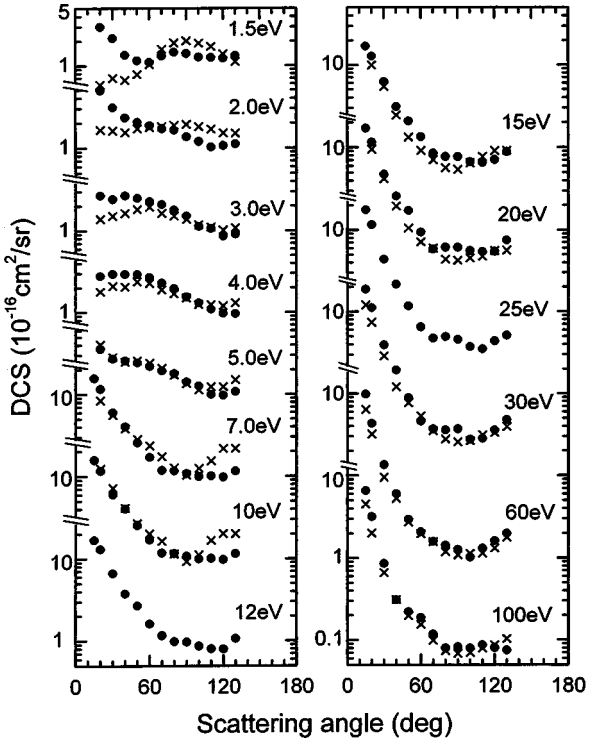

FIG. 3. Comparison of DCSs for allene (●) and ethylene (×) [2].

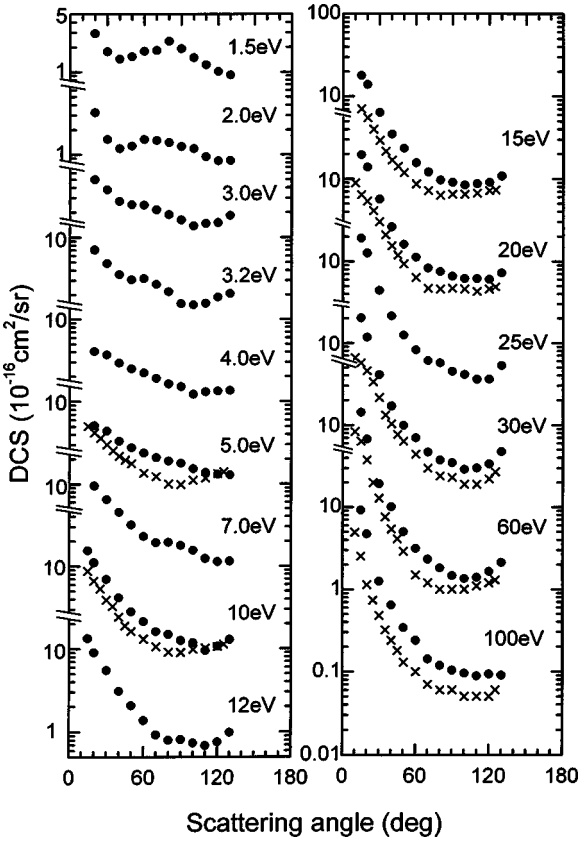

FIG. 4. Comparison of DCSs for propyne (●) and acetylene (×) [4].

i.e., double- and triple-bond region. The deviation in the smaller scattering angle for propyne and C_2H_2 should be due to the fact whether the molecule has a permanent dipole moment or not. For allene and C_2H_4, the deviation at smaller angles is much less because the dipole moment of allene is smaller by a factor of 3 than that of propyne. The CMS results show much conspicuous difference in DCSs among these molecules, particularly in the scattering angle below 20°. Since DCSs for C_2H_2 and C_2H_4 molecules, and allene and propyne are found to be quite different as discussed, good agreement seen for DCSs for allene and C_2H_4, and propyne and C_2H_2 at larger scattering angles suggest that there is the bonding effect, or the effect of the local charge distribution within a molecule, and as the scattering angle decreases, the bonding effect weakens and a long-range interaction takes over the role.

B. Vibrational excitation

As mentioned in the experimental procedure, it was in general not possible to separate the individual vibrational modes with the available energy resolution in the case of large molecules. But, some features for the vibrational modes can be predicted by applying the unfolding procedure to the observed composite energy-loss spectra, even in the case of 10 and 11 vibrational excitations such as in allene and propyne. Resonant electron scattering offers not only a direct means of probing normally unoccupied molecular orbitals but also accounts for the observed selectivity of the preferentially excited vibrational modes. According to Andrick and Read [15], electron scattering from C_3H_4 may be illustrated for a resonance process,

$$e + M \rightarrow M^- \rightarrow M^* + e,$$
$$\Gamma_{w1} \quad \Gamma_i \qquad \Gamma_{\mathrm{TNI}} \qquad \Gamma_f \qquad \Gamma_{w2}$$

where the initial vibronic state of the molecule M is the ground state with the symmetry Γ_i, and M^* and M^- present the final excited state of the symmetry Γ_f and the negative-ion resonance of the symmetry Γ_{TNI}, respectively. Here Γ_{w1} and Γ_{w2} are the initial and the final angular momentum of an incident and a scattered electron, respectively.

1. Allene

Figures 5(a)–5(d) show several energy-loss spectra of allene measured with primary energies 2, 5, 7, and 20 eV at a scattering angle 90°. At 2 and 7 eV, the energy-loss spectra for vibrational excitations are apparently enhanced, but no such feature is found in the nonresonant energy region at 5 and 20 eV. Within the present energy resolution, three prominent compound peaks are observed at 0.12 eV (C—H bending vibrations, mainly, ν_4), 0.24 eV (C—O stretching vibrations ν_6), and 0.38 eV (C—H stretching vibrations $\nu_1+\nu_5+\nu_8$) at 2 eV, which are presented as ν_b, ν_s, and $\nu_{s'}$, respectively, in Fig. 5(a). At 7 eV, the energy-loss peaks near 0.24 eV have disappeared and a new feature emerges at 0.17 eV (C—H bending vibrations). The corresponding excitation functions for the three energy-loss peaks ν_b, ν_s, and $\nu_{s'}$ are represented in Figs. 6(a)–6(c). There are two resonance regions centered near 2.1 and 11 eV for ν_b and ν_s, as well as

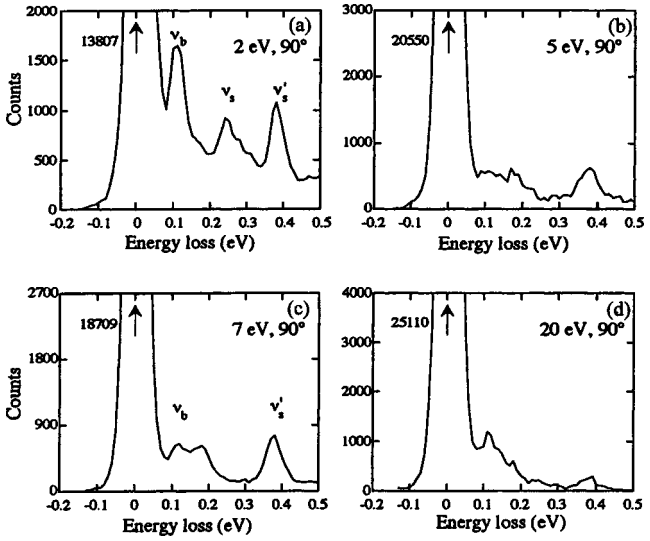

FIG. 5. Energy-loss spectra for vibrational excitations at different incident energies for allene.

near 2.1 and 7 eV for $\nu_{s'}$, respectively. The former profile shows a sharp resonance of intermediate lifetime, while the latter is very broad and shifted to lower incident energy. These are very similar to those of ethylene [3], propylene [1], and even to oxygen (O═O) [24], which have the double bonding structure characteristics. In the prototype hydrocarbon molecule C_2H_4, its ground electron configuration and the unoccupied orbitals are $(1a_g)^2(1b_{1u})^2(2a_g)^2(2b_{1u})^2(1b_{1u})^2(3a_g)^2(1b_{3g})^2(1b_{3u})^2(1b_{2g}\pi^*)^0(4a_g)^0$. Walker, Stamatoric, and Wong [3] concluded that the first sharp resonance at 1.8 eV, formed by accommodation of the

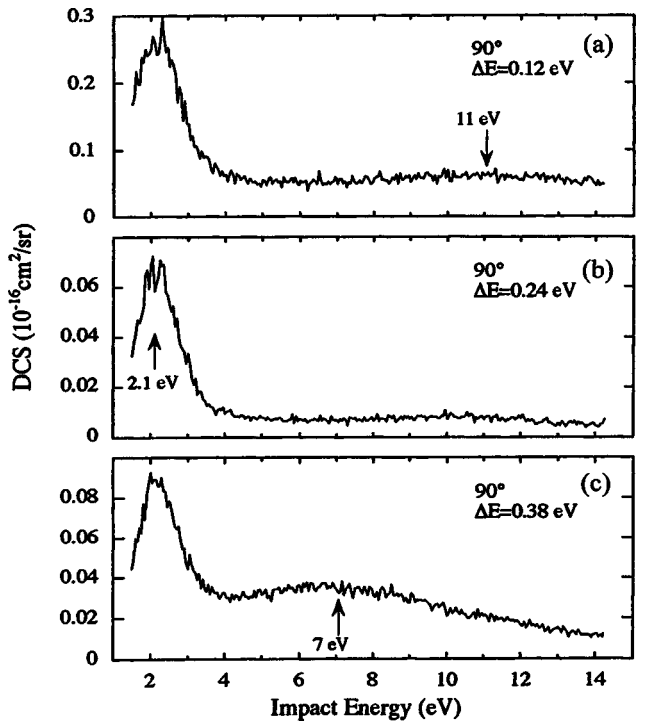

FIG. 6. Incident electron energy dependence for the vibrational excitations at the three prominent loss peaks for allene.

TABLE II. Representations of the symmetry species of the states involved in the resonances for allene.

Γ_{TNI}	Vibrational mode	Allowed[†]
e	ν_1-ν_7	1, 2
a_1	ν_1-ν_3	0, 2

[†]Of the outgoing wave in a molecular fixed system.

incident electron in the lowest-unoccupied molecular orbital (LUMO) $1b_{2g}(\pi^*)$, was accounted for by a $^2B_{2g}$ shape resonance, the broad feature being a ^2A_g state formed by trapping the incident electron in the next higher $4a_g$ orbital.

For allene, by analogy, we postulate that the first sharp peak happens through a resonance in which the negative-ion state consists of a ground-state molecule plus an electron temporarily trapped in the LUMO $3e$ (π^*) or the next higher orbital with the different symmetry $5a_1$. As mentioned above these states were predicted previously by electron-impact spectroscopy [12]. Furthermore, molecular structure calculations using the Gaussian program have proved that the LUMO and the higher orbital are assumed to have e and a_1 representations. Note here that because the next higher orbitals can be expected to arise from the eight excited states, the next higher states also belong to the same symmetry as the LUMO. Therefore, the e symmetry representation presents not only the lower shape resonance but also the broader, higher one.

According to the selection rules postulated by Wong and Schulz [24], the symmetries of the preferentially excited vibrational modes, into which the intermediate resonant states decay, can be given by the direct product as follows: $\Gamma_i \times \Gamma_\mu \times \Gamma_f \in A_1$, where A_1 is totally symmetric representation and $\Gamma_\mu = \Gamma_{\mathrm{TNI}} \times \Gamma_{\mathrm{TNI}}$ is due to general assumptions about electron charge distributions in the resonant orbitals. Hence, the number of vibrational modes can be reduced in either case, the e symmetry (A) or the a_1 symmetry (B), as shown in Table II. Then, based on this symmetry analysis, a least-squares-fitting procedure [25] is employed to elucidate the intensity of the individual mode at 2 and 7 eV as shown in Figs. 7(a) and 7(b) and Figs. 8(a) and 8(b), respectively. These clearly illustrate that the first vibrational peak can only be reproduced by taking into account vibrational modes ν_4, ν_5, and ν_{11}, all of which belong to representation e, except in case where the two other peaks contain more complicated contributions for higher harmonics and mixed vibrational transitions. Despite the 11 fundamental vibrational modes in which the allene molecule can vibrate, only a few modes have been observed. Note here that the ν_{11} mode is not listed in Table I. As pointed out by Wong and Schulz [26]; Walker, Stamatoric, and Wong [3]; Benott and Abouaf [27]; and Gallup [28], a component of a_1 symmetry is admixed to the resonances due to the interference of the direct nonresonant and resonant scattering. For the ν_8, ν_9, ν_{10}, and ν_{11} modes, the form $\Gamma_\mu = (e+a_1)\times(e+a_1) = 2a_1 + b_1 + b_2 + 2e$ is obtained, while for the a_1, $\Gamma_\mu = (a_1+a_1)\times(a_1+a_1) = 4a_1$.

Finally, according to the angular-correlation theory [15], the symmetry representation Γ_{w2} of the scattered electron is again deduced from the direct product rule ($\Gamma_{w2} \times \Gamma_f$

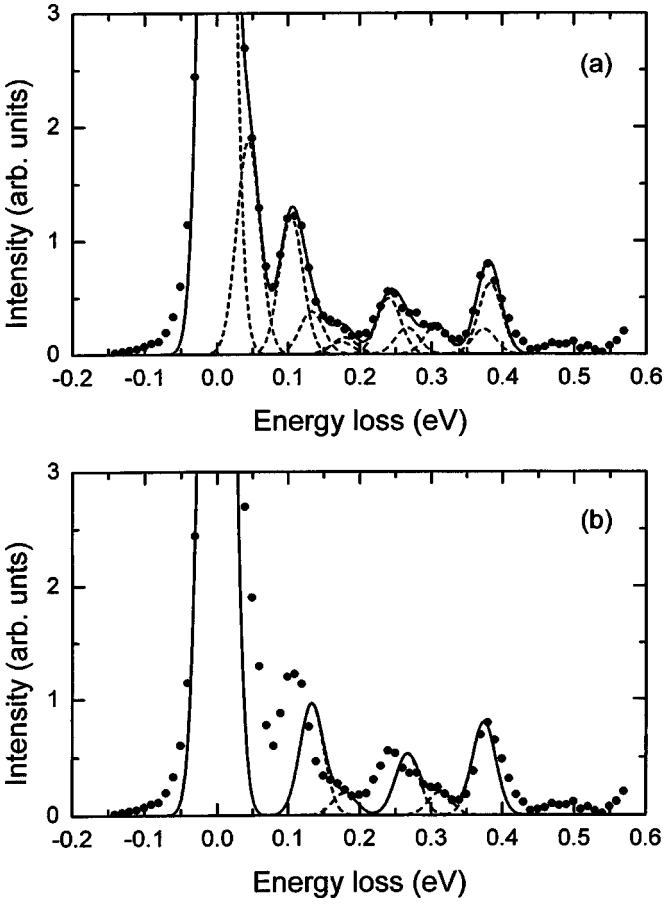

FIG. 7. State-resolved energy-loss spectra by deconvoluting the energy-loss peaks at 2 eV for allene. (a) Assuming that $\Gamma_{\mathrm{TNI}}=e$ and (b) $\Gamma_{\mathrm{TNI}}=a_1$.

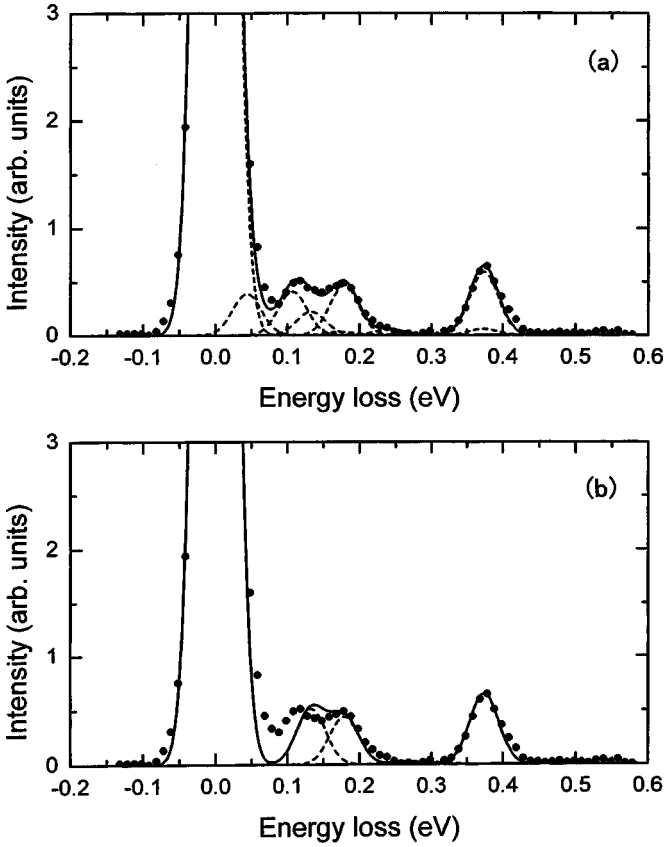

FIG. 8. State-resolved energy-loss spectra by deconvoluting the energy-loss peaks at 7 eV for allene. (a) Assuming that $\Gamma_{\mathrm{TNI}}=e$ and (b) $\Gamma_{\mathrm{TNI}}=a_1$.

$=\Gamma_\mu$), so that $\Gamma_{w2}=e$ for (*A*) or $\Gamma_{w2}=a_1$ for (*B*). Hence, in either case (*A*) or (*B*), the scattered wave is expressed in spherical harmonics associated with Legendre functions [28,29] in a target fixed-coordinate system whose the allowed angular-momentum terms are listed in Table II. After transforming the fixed-coordinate frame to the laboratory frame, the angular distribution is characterized by a series of the Legendre functions $P_k(\cos\theta)$ with a maximum value of $k_{\max}=4$. Because many peaks in the spectra overlap, even this procedure may still lead to mathematical instabilities. Therefore, the angular distributions in the decomposed ν_4, ν_5, and ν_6 are shown in Figs. 9(a)–9(d) only for a reference. The angular distribution for the ν_4 mode at 2.1 eV shows a weak minimum 50°–60° followed by a broad hump centered around 90°, characteristic of a resonant *d*-wave scattering, while a slight *p*-wave feature emerges at 7 eV. This is very similar to that of ethylene. It seems that other two angular distributions cannot be reproduced by one single partial wave but that several waves must be taken into account to the resonant part of the scattering amplitudes.

2. Propyne

Energy-loss spectra for vibrational excitation in propyne are shown in Figs. 10(a)–10(c) with primary energies 3.2, 7, and 10 eV at a scattering angle 90°. While the general energy-loss peak profiles are similar to each other, the vibrational features are enhanced to be sharper at 3.2 eV. With the present measurements as mentioned above, it was not possible to investigate the excitations of all the 10 individual normal vibrations for either the propyne or allene molecules. The two very weak peaks are separated from the elastic peak at 0.17 eV (C—H bending, mainly, ν_4), 0.27 eV (C≡C stretching, mainly, ν_3), and 0.37 eV (C—H stretching ν_6), which are indicated as ν_b, ν_s, and $\nu_{s'}$ in Figs. 10(a)–10(c), respectively. Figures 11(a)–11(c) present the energy dependence for differential cross sections of three peaks ν_b, ν_s, and $\nu_{s'}$ at a scattering angle 90°. Two resonance regions centered near 3.2 and 7.5 eV are evident in their energy dependence curves for the ν_b, ν_s, and $\nu_{s'}$ modes at a scattering angle 90°. In prototype hydrocarbon acetylene (C_2H_2), a similar resonance feature, shifted to lower energies, was observed at 2.5 eV by Refs. [4], [8], [14], and at 6 eV by Andric and Hall [30]. The prominent resonance at 2.5 eV were assigned to $^2\Pi_g$ symmetry similar to nitrogen (N≡N) that is isoelectronic to C_2H_2.

In accordance with allene, the LUMO and the next higher orbital for propyne in which the incident electron is temporally captured are postulated to have $3e$ and a_1 symmetries from the electron-impact spectroscopy [14], as well as from the molecular structure calculation based on the Gaussian program. The selection rule for vibrational excitation via

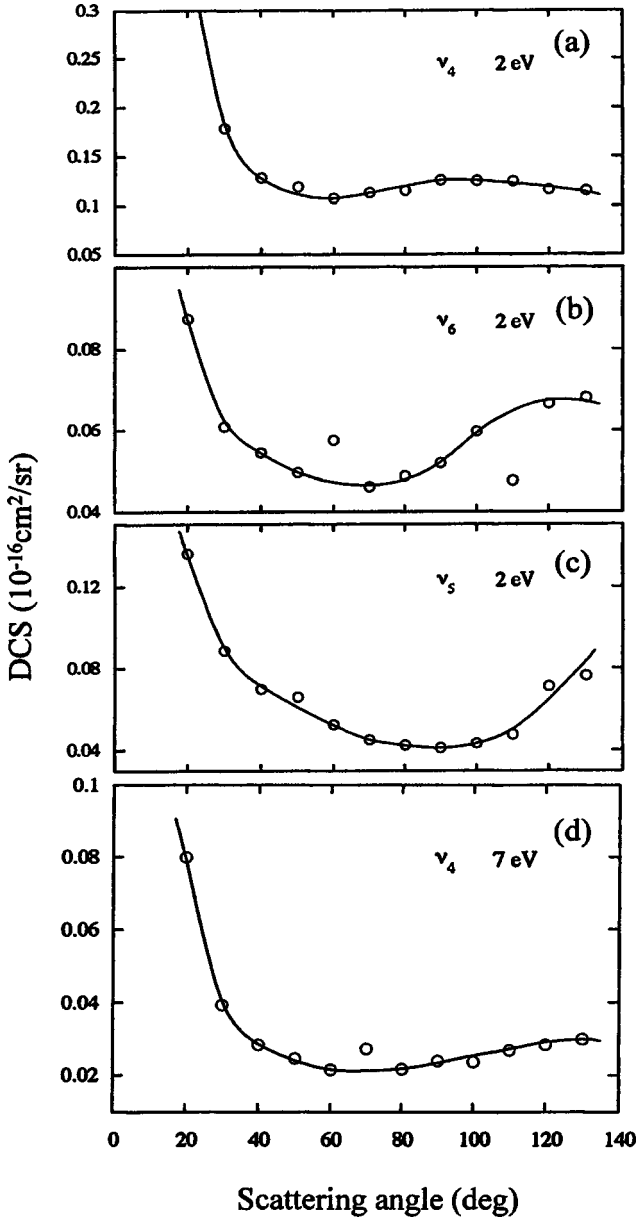

FIG. 9. Angular distributions for the individual vibrational transitions at the resonant energies for allene.

resonances and the angular-correlation theory have been applied to the vibrational excitation only via the 3.2-eV resonance. The allowed vibrational modes and angular-momentum terms are listed in Table III. Whereas in either propyne or allene, the LUMO is represented by the same symmetry $3e$, this symmetry for propyne is lower than that of allene because propyne belongs to C_{3v} point group. This leads not to reduce the number of the allowed vibrational modes. In the case of $\Gamma_\mu = e$, the allowed vibrational modes are classified by the allowed angular-momentum terms for the scattered electron in Table III. Note here that the cross section for the broad resonance around 7.5 eV is too small to analyze. From this analysis, to investigate strong selectivity in vibrational excitation via the shape resonance in some detail, vibrational modes tentatively decomposed are illustrated in Figs. 12(a) and 12(b). It is obvious that the shoulder

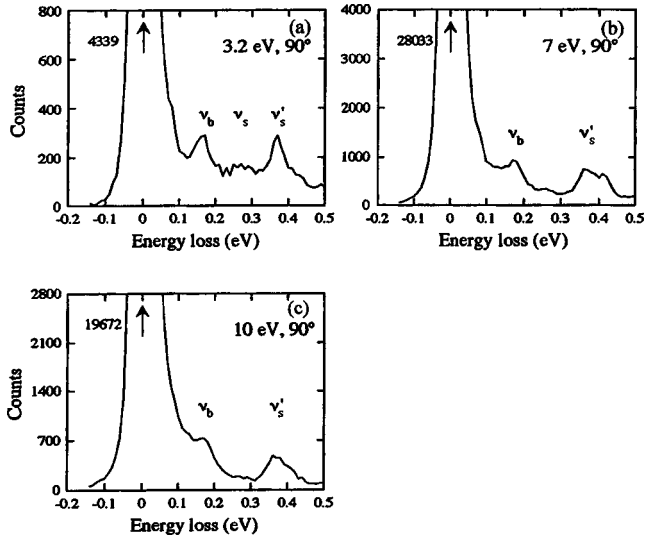

FIG. 10. Energy-loss spectra for vibrational excitations at different incident energies for propyne.

at the left of the first vibrational peak can only be accounted for by including vibrational modes ν_9 and ν_{10}, which belongs to the e symmetry. Here, it should be noticed that the ν_9, ν_3, and ν_6 vibrations are predominantly excited of the 10 normal modes. Furthermore, the corresponding angular distributions of the scattered electrons are shown in Figs. 13(a)–13(c), which could, in general, give much detailed information on the resonances. The DCSs for the ν_9 mode show characteristics of $P_4(\cos\theta)$ with a resonant d-wave scattering; for the ν_3 mode, $P_5(\cos\theta)$ with a f wave being predominantly excited; and for the ν_6 mode, $P_5(\cos\theta)$ with

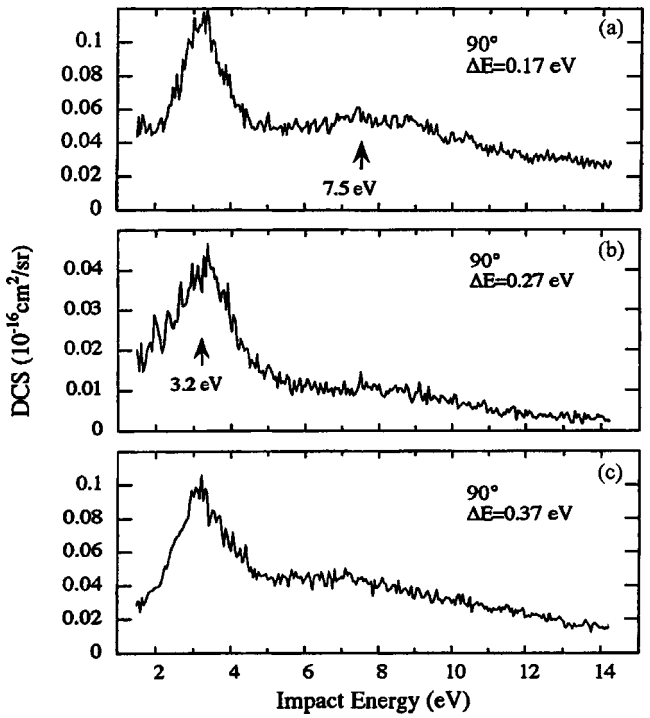

FIG. 11. Incident electron energy dependence for the vibrational excitations at the three prominent loss peaks for propyne.

TABLE III. Representations of the symmetry species of the states involved in the resonances for propyne.

Γ_{TNI}	Vibrational mode	Allowed
e	ν_1-ν_5	1, 2
	ν_6-ν_{10}	0, 1, 2
a_1	ν_1-ν_5	0, 1

some mixed of *p*, *d*, and *f* waves, respectively. These are consistent with the allowed angular-momentum terms listed in Table III. Again, the general trends are very similar to acetylene for both energy and angular dependences for the vibrational excitations.

A point to stress considering these resonance processes is a common feature about the scattering being dominated by two resonance regions in which the vibrational excitations are selectively enhanced in the double- and triple-bonded hydrocarbon molecules such as C_2H_4, C_3H_6, C_2H_2, and C_3H_4. Likewise, from the present results, the sharp resonance feature in the lower-energy region can be explained systematically by a temporary trapping of the electron in the $3e\pi^*$ orbital of the C—C bond. While one broad maximum of three single-bonded saturated hydrocarbons (CH_4, C_2H_6, C_3H_8, and so on) occurs around the same position of 7.5 eV, which is due to a capture of the electron in the σ^* antibonding orbital of the C—H bond.

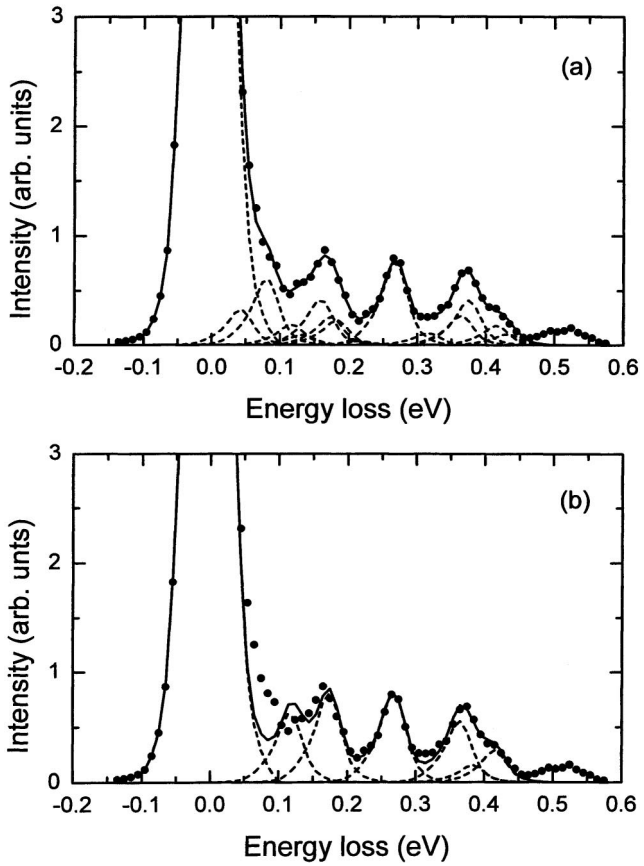

FIG. 12. State-resolved energy-loss spectra by deconvoluting the energy-loss peaks at 3.2 eV for propyne. (a) Assuming that $\Gamma_{TNI}=e$ and (b) $\Gamma_{TNI}=a_1$.

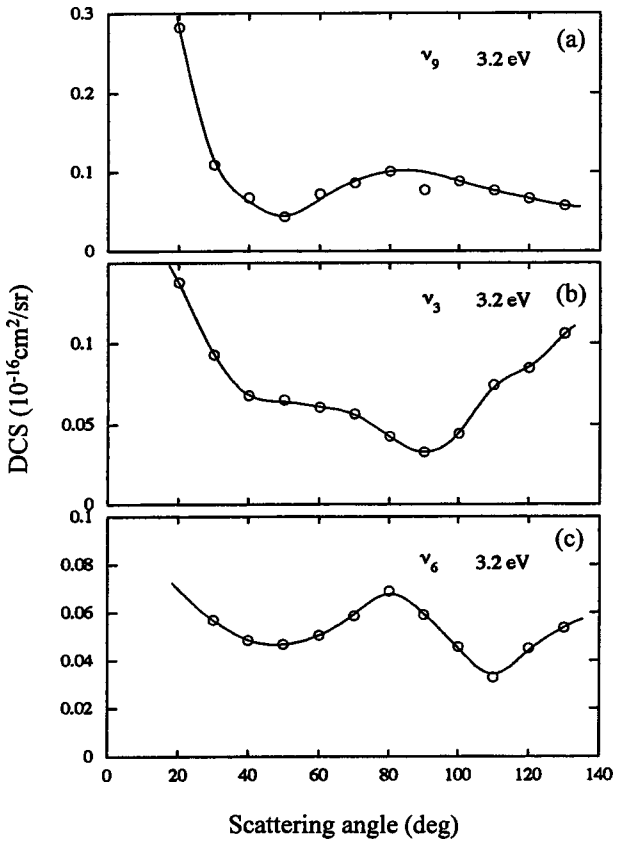

FIG. 13. Angular distributions for the individual vibrational transitions at the resonant energy for propyne.

IV. CONCLUSIONS

Extending the previous study of the prototype double- and triple-bonded hydrocarbon C_2H_4 and C_2H_2 molecules to the isomers C_3H_4, absolute elastic DCSs have been determined at incident energies of 1.5 to 100 eV and scattering angles from 15° to 130°. These results are very similar to each other at incident energies above 5 eV, while some differences emerge below 5 eV suggesting rather strong isomer effects. These differences mainly depend on the strength of a permanent dipole moment, a resonance, or both. A comparison of the present allene and propyne with C_2H_2 and C_2H_4 molecules suggests the bonding effect, or the effect of charge distribution of a molecule, at least, at larger scattering angles above 40° and at higher impact energy above 20 eV. To the best of our knowledge, these two effects are the first observation of these kinds, and are important for basic physics as well as for applications.

In addition, the present results for state-resolved vibrational excitations obtained by deconvoluting energy-loss spectra provide detailed information on the resonant states. In spite of the complexity of the molecules, the selection mechanisms can account for quite simple excitation schemes at the resonances. The $3e$-type (C═C, C≡C; π^*) resonances are assigned to be located at 2.1 eV in allene and at 3.2 eV in propyne, respectively. It is confirmed that the sharp resonances located near 2 eV are a common feature of the double- and triple-bonded hydrocarbon molecules. However, comparing allene with propyne from viewpoint of the iso-

mer, whereas several differences are noticeable, there is less in common between the two molecules.

ACKNOWLEDGMENTS

The authors are much indebted to Professor S. J. Buckman and Dr. R. J. Gulley for reading the manuscript and giving helpful suggestions. H.T. also gratefully acknowledges the warm hospitality extended to him by Professor S. J. Buckman during a sabbatical at the Australian National University, Canberra where this paper was prepared. The work was supported in part by the Grant-in-Aid from the Ministry of Education, Science, Technology, Sport and Culture, Japan Society for Promotion of Science (JSPS), and National Institute for Fusion Science, Japan (MK).

[1] L. Boesten, T. Takagi, H. Tanaka, M. Kimura, H. Sato, and M.A. Dillon, in *Abstract Papers of the 18th International Conference on the Physics of Electronic and Atomic Collisions* (Aarhus University, Denmark, 1993), p. 264.
[2] B. Mapstone and W. R. Newell, J. Phys. B **25**, 491 (1992).
[3] I. C. Walker, A. Stamatoric, and S. F. Wong, J. Chem. Phys. **69**, 5532 (1978).
[4] K.-H. Kochem, W. Sohn, K. Jung, H. Ehrhardt, and E. S. Chang, J. Phys. B **18**, 1253 (1985).
[5] M. A. Khakoo, T. Jayaweera, S. Wang, and S. Trajmar, J. Phys. B **26**, 4845 (1993).
[6] C. R. Bowman and W. D. Miller, J. Chem. Phys. **42**, 681 (1965).
[7] H. H. Brongersma, J. A. van der Hart, and C. J. Osterhoff, Nobel Symp. **5**, 211 (1967).
[8] D. F. Dance and I. C. Walker, J. Chem. Soc., Faraday Trans. 2 **70**, 1426 (1974).
[9] K. K. Jung and M. A. M. Kadisch, J. Phys. B **14**, 3289 (1981).
[10] H. Deutsch, K. Becker, R. K. Janev, M. Probst, and T. D. Maerk, J. Phys. B **33**, L865 (2000).
[11] H. Nishimura and H. Tawara, J. Phys. B **24**, L363 (1991).
[12] O. A. Mosher, W. M. Flicker, and A. Kuppermann, J. Chem. Phys. **62**, 2600 (1975).
[13] W. M. Flicker, O. A. Mosher, and A. Kuppermann, J. Chem. Phys. **69**, 3311 (1978).
[14] E. H. Van Veen and F. L. Plantenga, Chem. Phys. Lett. **38**, 493 (1976).
[15] D. Andrick and F. H. Read, J. Phys. B **4**, 389 (1971).
[16] H. Tanaka, T. Ishikawa, T. Masai, T. Sagara, L. Boesten, M. Takekawa, Y. Itikawa, and M. Kimura, Phys. Rev. A **57**, 1798 (1998).
[17] S. K. Srivastava, A. Chutjian, and S. Trajmar, J. Chem. Phys. **63**, 2659 (1975).
[18] Gases used for allene and propyne were manufactured by, and purchased from the SymQuest Labs, USA, and INTERGAS, UK, respectively.
[19] M. Kimura and H. Sato, Comments At. Mol. Phys. **26**, 333 (1991).
[20] *CRC Handbook of Chemistry and Physics*, 69th Ed., edited by R.C. West (CRC, New York, 1988).
[21] T. Shimanouchi, *Tables of Molecular Vibrational Frequencies*, Natl. Bur. Stand. Ref. Data Ser., Natl. Bur. Stand. (U.S.) Circ. No. 39 (U.S. GPO, Washington, D.C., 1972), Vol 1.
[22] C. Fridh, J. Chem. Soc., Faraday Trans. 2 **74**, 2193 (1978).
[23] R. Merz and F. Linder, J. Phys. B **31**, 4663 (1998).
[24] S. F. Wong and G. J. Schulz, Phys. Rev. Lett. **31**, 969 (1973).
[25] M. A. Dillon, L. Boesten, H. Tanaka, M. Kimura, and H. Sato, J. Phys. B **26**, 3147 (1993).
[26] S. F. Wong and G. J. Schulz, Phys. Rev. Lett. **35**, 1429 (1975).
[27] C. Benott and R. Abouaf, Chem. Phys. Lett. **123**, 134 (1986).
[28] G. A. Gallup, Phys. Rev. A **34**, 2746 (1986).
[29] F. H. Read, J. Phys. B **1**, 893 (1968).
[30] L. Andric and R. I. Hall, J. Phys. B **21**, 355 (1988).